The simulation of a plane-concave Fabry-Perot micro-cavity

THESIS

submitted in partial fulfillment of the
requirements for the degree of

BACHELOR OF SCIENCE
in
PHYSICS

Author :	S. Szkudlarek
Student ID :	s1663569
Supervisor :	Dr. Wolfgang Löffler
2^{nd} corrector :	Prof. Harold Linnartz

Leiden, The Netherlands, July 10, 2019

The simulation of a plane-concave Fabry-Perot micro-cavity

S. Szkudlarek

Huygens-Kamerlingh Onnes Laboratory, Leiden University
P.O. Box 9500, 2300 RA Leiden, The Netherlands

July 10, 2019

Abstract

A plane-concave Fabry-Perot micro-cavity model within COMSOL has been built. The design parameters, geometry and mesh of the 2D model have been successfully implemented and meet the design criteria. he solution of analytic model which describe the system had determined the resonant frequencies. In the study of the model with the use of a frequency sweep a number of resonant modes were found. The modes corresponding to the integer value N=2 & N=6 displayed modes which mostly likely describe physical modes. In addition to the correct field distributions, they also display resonant peaks in the spectrum of the 2D model.

Contents

Part I
Introduction

Quantum is a term which we can not miss present day. It is a field within physics which houses many mysteries, yet possibly houses more potential than we could ever expect. In the next decades these mysteries will unfold, new technology will emerge and break throughs will be made.

In many cases the understanding of physical phenomenon at micro-scale will be fundamental in the creation and understanding of various quantum principles. For example the scaling of quantum networks or the creation of a universal quantum simulator [1]. However in order to create these applications fundamental understanding of the quantum physics involved will be required. Moreover lab research of this microscopic world is not realized without extensive analytic and numerical analysis.

For that reason our goal is to simulate a plane-concave Fabry-Perot micro-cavity model, to gain a better understanding of the interactions of the photons within the micro-cavity. In addition the effects between photons and certain quantum emitters could be studied as this offers a rich field of applications in the creation of new quantum technologies [2].

Furthermore the high reflective mirrors are constructed with the use of Distributed Bragg Reflectors (DBR).These Distributed Bragg Reflectors are structures composed of multiple thin films with varying refractive indexes. The spacing and the curvature of these DBRs will determine the resonant frequencies of the system. These frequencies can be evaluated by considering the theory of light interferometry in these systems. Thus to gain a better understanding of the setup as a whole it will be important to investigate the analytic theory of such systems. The results found by the analytic theory can then be compared to numerical simulations preformed in COMSOL.

Moreover the setup will be constructed and evaluated with the use of COMSOL multi-physics software. In order to simulate field distributions with the aim to find resonant modes which are representations of physical phenomenon. Furthermore the aim will be to ensure that the geometry of the setup will not break when varying the design parameters of the system. An example of such a parameter is the curvature of the mirror or the wavelength of the incoming electric field. Lastly there will also be the possibility to change the distance of the air-gap (cavity length). The implementation of the these design parameters will ensure that the simulation build can be used to preform simulations which can easily be adapted to match the design parameters of the lab setup.

Creating the plane-concave Fabry-Perot Micro-Cavity setup in the COMSOL

multi-physics environment was a process which consisted of a number of steps. Initially the setup was created with perfect mirrors and thus due to the perfect conditions within the cavity was simple to create and compare the results to the theory. However when moving to the curved geometry with DBR's certain issues arose in the creation of the mesh. This resulted in long simulation times and large sets of data.

In the end this thesis has resulted in a COMSOL model for the simulation of a plane-concave Fabry-Perot micro-cavity setup with Distributed Bragg Reflectors and variable curvature.

Part II
Theory

1 Fabry-Perot

1.1 Fabry-Perot Interferometer Setup

A Fabry-Perot interferometer is a linear optical resonator. The setup consists of two identical partially reflective mirrors separated by a distance l. This causes the space between the mirrors to to behave as an optical cavity or optical resonator. The resonance within a cavity with fixed length (l) is dependent on the wavelength of the incoming light. Figure 1 is a sketch of a simple Fabry-Perot interferometer setup [3].

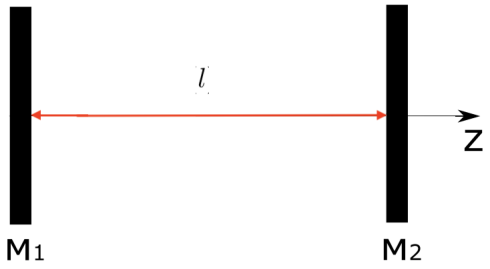

Figure 1: Fabry-Perot Setup (Simple) - Mirrors separated by a distance l

Considering the transmission spectrum as a function of wavelength it becomes apparent that this spectrum exhibits sharp transmission peaks which correspond to the resonant modes of the interferometer setup. These resonant modes are described by the free spectral range, finesse and quality factor (Q-factor) of the system.

Often used as an optical spectrometer this setup allows the investigation of wavelength depend properties of light. However in the Quantum Optics group the aim will be to investigate the field distributions within the cavity. In order to enhance the interactions of light with for example quantum dots and other quantum emitters. The field distributions mentioned are described by Gaussian beam profiles, from which the stability criterion of the cavity can be established.

Furthermore the fundamental theory of the simple Fabry-Perot setup allows a better understanding of the tunable micro-cavity we aim to simulate. A de-

tailed description of this theory is given below. In addition the concepts for the description of the resonance modes are also discussed in the following section.

1.2 Fabry-Perot Interferometer Theory

In a Fabry-Perot setup as described above the initial incident wave amplitude U_0 is passed through the first partially reflecting mirror. The transmitted amplitude is then a fraction t_1 of the incident wave amplitude. As the wave passes through the cavity it is undergoes two reflections for every round trip made in the cavity. These reflections result in a reflected wave amplitude being a fraction r^2 of the initial transmitted amplitude ($U_0 t_1$) for every round trip made. In addition to the change in amplitude we find a phase shift depend on the distance between the mirrors (l) and the angle of incidence (θ) with respect to the normal, the phase change which occurs in one round trip is then equal to $k \cdot 2l \cdot cos(\theta)$. The effects of these round trips on the amplitude and phase of the incident light are shown in the figure below.

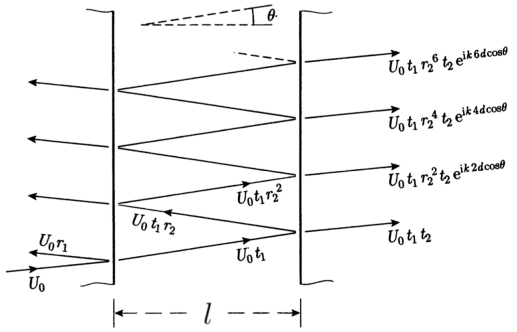

Figure 2: Fabry-Perot interferometer in which the round trip and transmission amplitudes are shown. Adaptation of Brooker fig. 5.1 [3]

As can be seen in the figure above the output of the Fabry-Perot setup is the sum of the wave amplitude fractions and phase shifts which have occurred as the light passed through the setup. These influences on the phase and amplitude are given by the following sum:

$$\sum_n U_0 t_1 t_2 (r^2 e^{ik2lcos(\theta)})^n \tag{1}$$

In this equation $n$is the index which represents the number of round trips, not the refractive index, t_1 is the transmitted amplitude fraction when passing

through the first mirror, t_2 is the transmitted amplitude fraction when passing through the second mirror. The last factor $|r^2|e^{ik2dcos(\theta)}$ is the contribution to the phase change and the reflected amplitude for every round trip.

We can denote the effects on the wave phase and amplitude in a more elegant manner by defining $R = |r^2|$ we find that we can replace the factor r^2 by $R \cdot e^{-i\alpha}$. This substitution will add a factor to the phase change which occurs with every round trip. Furthermore we can also introduce the factor $\delta = k2lcos(\theta) - \alpha$. Substituting these expressions into equation 1 allows us to simplify the sum to [3]:

$$\sum_n I_0 t_1 t_2 (Re^{ik2lcos(\theta)-i\alpha})^n = \sum_n I_0 t_1 t_2 R^n e^{i\delta n} \tag{2}$$

Working out the sum we find the following equation:

$$U_{out} = U_0 t_1 t_2 (1 + Re^{i\delta} + R^2 e^{i2\delta} + ...) = \frac{U_0 t_1 t_2}{1 - Re^{i\delta}} \tag{3}$$

We have an expression for the wave amplitude after the light has passed through the Fabry-Perot setup. The phase factor contributed by α arose from the theory however in reality it is negligible and for that reason will be left out in further sections.

1.3 Fabry-Perot Resonance

In our case the mirrors on either side of the Fabry-Perot cavity setup will be identical and thus $t_1 = t_2$ with this in mind we can define $T = |t_1 t_2| = 1 - R$, such that all the light which is not transmitted is reflected and vice versa. The factor R is thus a measure for the internal reflectivity of the cavity. In addition we know that passing through the cavity setup the light undergoes half a phase shift equal to half the phase shift of a full round trip. Thus the equation above can be written as:

$$\frac{U_{out}}{U_0} = \frac{Te^{i\frac{\delta}{2}}}{1 - Re^{i\delta}} = \frac{(1-R)e^{i\frac{\delta}{2}}}{1 - Re^{i\delta}} \tag{4}$$

From this is equation it becomes clear that the maximum transmission will occur when $e^{i\frac{\delta}{2}} = e^{i\delta}$ and the minimum transmission when $e^{i\frac{\delta}{2}} = 1$ and $e^{i\delta} = -1$, this minimum case will not be looked at in further detail. This will result in the following:

$$(\frac{U_{out}}{U_{in}})_{max} = \frac{1-R}{1-R} = 1; \qquad (\frac{U_{out}}{U_{in}})_{min} = \frac{1-R}{1+R} \tag{5}$$

This is the case if the phases match and thus $e^{i\delta} = e^{i\frac{\delta}{2}}$. This statement holds

when $\delta = N \cdot 2\pi$, this result can be interpreted in the following manner namely that for a certain frequencies the system will have maximum transmission due to interference of the electromagnetic wave. Moreover δ depends on the length of the cavity (l), the wavenumber (k) and the angle of incidence (θ) with respect to the normal.

$$\delta = k \cdot 2l \cdot \cos(\theta) = k \cdot 2l$$

In our case the angle of incidence is equal to 0 and thus the factor $cos(\theta)$ is equal to 1 and we end up with the following equation:

$$k \cdot 2l = N \cdot 2\pi \tag{6}$$

The wavenumber k is related to the wavelength (λ) in the following way $k = \frac{\omega}{c} = \frac{2\pi \cdot v}{c} = \frac{2\pi}{\lambda}$. Thus this equation can be written in terms of wavelength and cavity length resulting in the following:

$$\lambda_N = \frac{2l}{N} \tag{7}$$

Note that this is the case when the medium within the cavity in which the light propagates has a refractive index $n = 1$. If this is not the case the equation above would need to be multiplied by a factor n. Furthermore this relations shows that in attempting to find the resonance modes within a cavity we can either vary the wavelength of the incoming light or we can vary the cavity length. The description of the Fabry-Perot cavity above is only valid for perfect mirrors without optical absorption. However in reality this is rarely the case.

Considering the resonance conditions given by equation 7 we find that $l = N \cdot \frac{\lambda}{2}$. Thus the cavity length must be a integer multiple of the half the wavelength of the incident light in order for the resonance conditions to be met. This principle results in the fact the we can monitor the resonance conditions of a cavity in order to determine small changes in the cavity length. Although this is not relevant in our case since the cavity length is a set parameter which we do not vary, it is a valuable concept which is used in other interferometer setups such as for instance LIGO.

1.4 Characterizing Fabry-Perot Resonance

1.4.1 Finesse

Thus far we have considered the input field and the output field of the system. This is however not the only relation we are interested in, we would also like to

consider the transmitted intensity as a fraction of the incident intensity. The ratio of transmitted intensity with respect to the incident intensity is equal to the square of the wave amplitude and phase change, thus we find:

$$\frac{I_{transmitted}}{I_{incident}} = \frac{|U_{out}|^2}{|U_0|^2} = (\frac{T}{1-R})^2 \frac{1}{1+\frac{4R}{(1-R)^2}\sin^2(\frac{\delta}{2})} \tag{8}$$

The prefactor $T/(1-R)$ is not of significant physical relevance as it is defined by the mirrors used in the setup. For this reason we can absorb it into the $I_{incindent}$ factor as followed, $I_{max} = I_{incident} \cdot (\frac{T}{(1-R)})^2$. Furthermore we introduce definition for finesse which is as followed $\mathcal{F} = \pi\sqrt{R}/(1-R)$ and can rewrite equation 8 as [3]:

$$\frac{I_{transmitted}}{I_{max}} = \frac{1}{1+4\frac{\mathcal{F}^2}{\pi^2}\sin^2(\frac{\delta}{2})} \tag{9}$$

From the equation above it becomes clear that the finesse factor introduced has an influence on the transmission spectrum of the interferometer.

Moreover considering the full width half maximum can be determined by evaluating $\frac{I_{trans}}{I_{max}} = \frac{1}{2}$ we know

$$4\frac{\mathcal{F}^2}{\pi^2}\sin^2(\frac{\delta}{2}) = 1; \qquad \sin^2(\frac{\delta}{2}) = \frac{\pi^2}{4\mathcal{F}^2}$$

$$\sin(\delta/2) = \pm\frac{\pi}{2\mathcal{F}} \tag{10}$$

Furthermore we know that $\delta = N \cdot 2\pi + \epsilon$ as we know that the fullwidth half maximum is close to the peak we know that ϵ will be small. Substituting this into equation 10 we find to following [3]:

$$\pm\frac{\pi}{2\mathcal{F}} = \sin(N \cdot \pi + \frac{\epsilon}{2}) = (-1)^N \sin(\epsilon/2)$$

thus we get

$$\epsilon = 2\arcsin(\pm\frac{\pi}{2\mathcal{F}})$$

Lastly utilizing the power series for arcsin and since ϵ is small we will find that $\epsilon = \pm\frac{\pi}{\mathcal{F}}$. Thus considering the FWHM along the δ axis we find that the FWHM is equal to $\frac{2\pi}{\mathcal{F}}$. This allows us to evaluate the distance between the N-th peak against the FWHM of 1 peak along the δ axis. From equation 7 we know that the N-th peaks will be spaced by a distance 2π on the δ axis. This results in the following expression [3]:

$$\frac{\text{Distance between Nth peak}}{\text{FWHM single peak}} = \frac{2\pi}{2\pi/\mathcal{F}} = \mathcal{F} \tag{11}$$

This expression shows the meaning of the parameter finesse ($\mathcal{F}$) which was introduced at the start of this section. Important to take away from this is the fact that narrow peaks result in a high finesse. Such that the finesse is a measure for the resolution of the peaks in the Fabry-Perot setup.

1.4.2 Free Spectral Range

The free spectral range ($\Delta\nu_{_{FSR}}$) is measure for the distance in wavelength or frequency between successive maxima or minima in a interferometer setup. In the case of a Fabry-Perot setup it defines the spacing between the transmission peaks of the system. In other words it is a value for the spacing and and resolution of the resonator modes of cavity setup. The free spectral range can be expressed in terms of either wavelength of frequency:

$$\Delta\lambda_{\text{FSR}} = \frac{\lambda^2}{2l \cdot n}; \qquad \Delta\nu_{_{FSR}} = \frac{c}{2l \cdot n} \tag{12}$$

Where n is the index of the material within the cavity, l is the length of the cavity, λ is the wavelength of the incident light and c is the speed of light. It becomes apparent that the expression of in terms of frequency is the inverse of the round trip time (T_R).

$$T_R = \frac{2l \cdot n}{c} = \frac{1}{\Delta\nu_{_{FSR}}}$$

The free spectral range, the FWHM (bandwidth, $\Delta\nu_{_{FWHM}}$) and the finesse ($\mathcal{F}$) are related by equation 11 and thus we find

$$\mathcal{F} = \frac{\Delta\nu_{_{FSR}}}{\Delta\nu_{_{FWHM}}}; \qquad \text{(Finesse)}=\frac{\text{(Free Spectral Range)}}{\text{(Full Width Half Maximum)}}$$

In the figure below shows how these characterizations of the Fabry-Perot cavity are related to the transmission spectrum of the setup.

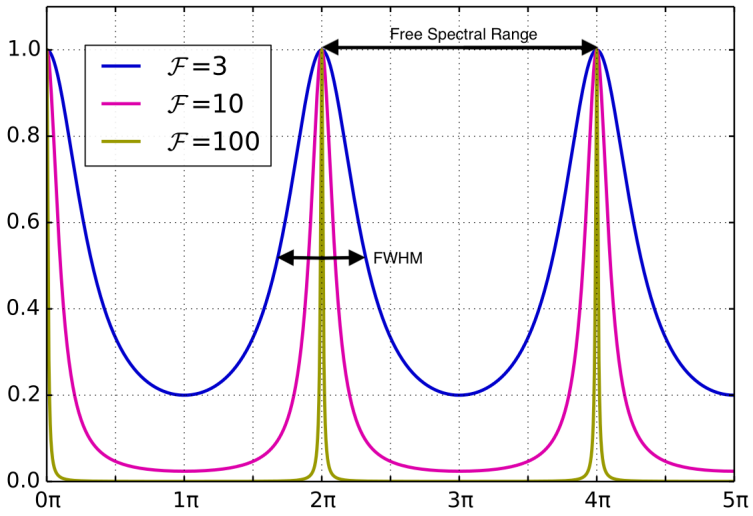

Figure 3: The transmission spectrum of a Fabry-Perot setup. In which the Free Spectral Range, the FWHM and the Finesse are also shown.[4]

1.4.3 Quality Factor

Lastly in the characterization of the Fabry-Perot setup we will introduce the quality factor (Q-factor). The Q-factor is an equivalent to the Finesse and thus a description for the quality of the resonator present in the cavity setup. To determine the expression for the quality factor first we introduce T_p which which is a measure for the lifetime of a photon in the cavity and is given by[5]:

$$T_P = \frac{T_R}{1-P_R} = \frac{1}{\Delta\nu_{_{FSR}}(1-P_R)} \approx \frac{1}{2\Delta\nu_{_{FSR}}(1-\sqrt{P_R})} \tag{13}$$

In which $P_R = R^2$ where R is again the internal reflectivity of the cavity. The expression for the finesse in these terms becomes $\mathcal{F} = \pi P_R^{\frac{1}{4}}/(1-\sqrt{P_R}) \approx \frac{\pi}{1-\sqrt{P_R}}$ in the case of large finesse. Rewriting equation 13 we find:

$$T_P = \frac{\mathcal{F}}{2\pi\Delta\nu_{_{FSR}}} = \frac{1}{2\pi\Delta\nu_{_{FWHM}}} \tag{14}$$

From the equation above we can determine the uncertainty relation relating T_P to $\Delta\nu_{_{FSR}}$ the relation being $T_P \cdot \Delta\nu_{_{FSR}} = \frac{1}{2\pi}$. The Q-factor is equivalent the ratio between the total stored energy within the system and the energy lost in a single cycle. This is denoted as follows[6]:

$$Q = 2\pi \cdot \nu_N \cdot T_P = \frac{\nu_N}{\Delta\nu_{_{FWHM}}} = N \cdot \mathcal{F}; \qquad Q = \frac{\text{(Total Stored Energy)}}{\text{(Energy Lost per Cycle)}} \quad (15)$$

In which $\mathcal{F}$ is the finesse and N the integer which labels the order of the resonant modes.

One of the reasons the Q-factor is important is due to the fact that it is the characterizing parameter of the system which can be determined from simply one resonance peak

2 Distributed Bragg Reflector

Thin-film interference is an important field of study when attempting to create highly reflective mirrors. A distributed Bragg reflector (DBR) is a structure of multiple thin films of varying refractive index. Each layer of this structure has a thickness (d_{DBR}) dependent on the wavelength of the incoming light (λ_0) and the refractive index of the material (n). The thickness of the layers is defined as [7, 8]:

$$d_{DBR} = \frac{\lambda_0}{4 \cdot n} \quad (16)$$

Where the refractive index n varies from layer to layer alternating between low and high indexes, with high indices on the edges of the cavity. This description corresponds to the definition of a quarter-wave mirror. Thus each pair of thin films with alternating reflective index constitutes a optical path length difference of $\frac{\lambda_0}{2}$ when passing through a pair of alternating index. In order to gain a better understanding of the functionality of a DBR we would like know the transmitted amplitude ($t \cdot U_0$) and the reflected amplitude ($r \cdot U_0$) which are both depend on the incoming field (U_0). This system is depicted in figure 4.

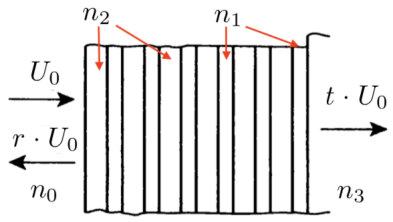

Figure 4: This is a sketch of a Distributed Bragg Reflector, which is made such that the system has the desired properties that meet the requirement for the simulation of the plane-concave Fabry-Perot Micro-Cavity setup. [3]

The reflectivity coefficient (r) for the in incoming field (U_0) can be found with the use of the following equation [9]:

$$r = \frac{n_0 n_2^{2m} - n_3 n_1^{2m}}{n_0 n_2^{2m} + n_3 n_1^{2m}} \tag{17}$$

In which n_0 is the index for the originating medium, n_3 is the index for the transmitting medium and n_1 & n_2 are the indices for the alternating quarter-wave layers. Lastly the factor m is the number of pairs the DBR is build from. Note the the reflectivity coefficient of the field intensity (I_0) is given by r^2. In addition the transmission of the system is given by $t = 1 - r - a$, where a is the factor which takes the absorption of the system into account.

For our understanding the propagation of the electro-magnetic field within the DBR is not of importance. The analysis of the light interaction within the DBR which results in a value for the transmitted amplitude ($t \cdot U_0$) and the reflected amplitude ($r \cdot U_0$) will be omitted. Due to the fact that it is not of further importance to the understanding of equation 17 which relates the reflectivity coefficient (r) to the refractive indices of the materials used to construct the quarter-wave layer DBR.

3 Gaussian Beam

In the understanding of the plane-concave Fabry-Perot Micro-Cavity setup the last important factor is the study of Gaussian beams. Gaussian beams are a from of electromagnetic radiation in which the transverse electric and magnetic field intensity profiles are given by a gaussian function. These profiles are described by a single parameter the minimum value of the beam width (w_0) (under the condition that the polarization and the wavelength are constant)[10]. The relation between the different parameter which describe the propagation of the Gaussian beam and w_0 are discussed in the following section.

As mention in the introduction of the Fabry-Perot cavity we need to determine the stability criterion for such a cavity. In the study of Gaussian beams we find that in the case of a plane-concave cavity setup the stability criterion reduce to the following equation [11]:

$$0 \leq (1 - \frac{l}{\mathcal{R}_{M_2}}) \leq 1 \tag{18}$$

In which l is the length of the cavity and $\mathcal{R}_{M_2}$ is the radius of curvature of the concave mirror in the setup. For equation 18 we can easy find the following requirement for the cavity length (l): $l \leq \mathcal{R}_{M_2}$[7].

Furthermore considering the fact that an arbitrary solution of the Helmholtz

equation ($\nabla^2 U(\mathbf{r}) + k^2 U(\mathbf{r}) = 0$) can be given by a combination of Hermite-Gaussian modes[12]. The aim will be to determine the solution of the Helmholtz equation for the boundary conditions imposed by the geometry of the plane-concave Fabry-Perot micro-cavity. Showing that these are indeed Gaussian beams as with the descriptive parameters depicted in figure 5. The solution of the Helmholtz equation under these condition is the following [6]:

$$U(\mathbf{r}) = A_0 \frac{w_0}{W(z)} \exp(-\frac{(x^2+y^2)^2}{W^2(z)}) \exp(-ikz - ik\frac{(x^2+y^2)^2}{2R(z)} + i\gamma(z)) \qquad (19)$$

Where the beam is traveling along the z-axis. Moreover $W(z)$ is the width of the Gaussian beam, z_0 is the Rayleigh range (the distance along the propagation axis between w_0 and $\sqrt{2}w_0$). The relation between the parameters are given by the following equations[13]:

$$z_0 = \frac{\pi w_0^2}{\lambda}; \qquad W(z) = w_0\sqrt{1 + (\frac{z}{z_0})^2}; \qquad R(z) = z(1 + (\frac{z_0}{z})^2)$$

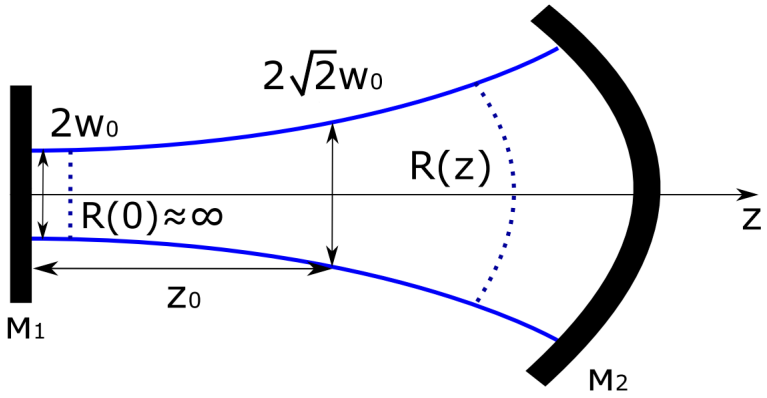

Figure 5: Gaussian beam in a cavity consisting of a planar mirror M_1 and curved mirror M_2 propagating along the z-axis. Smallest width of this Gaussian beam isw_0, its Rayleigh range is z_0 and its radius of curvature is $\mathcal{R}(z)$. [6]

In this description the origin of the Gaussian wave ($z = 0$) is set to the location where it can be described as a planar wave ($\mathcal{R}_{M_1} = \infty$), note that at this location the beam width is w_0. Conform to the geometry of the system the Gaussian mode which is stable within the resonator and hence the beam waist at the DBR interfaces are also stable. The beam waist at M_1 (w_0) and at

$M_2(w_1)$ are as follows[7]:

$$w_0 = \sqrt{\frac{\lambda_0}{\pi}}(l \cdot \mathcal{R}_{M_2} - l^2)^{\frac{1}{4}}; \qquad w_1 = \sqrt{\frac{\lambda_0 \mathcal{R}_{M_2}}{\pi}}(\frac{\mathcal{R}_{M_2}}{l} - 1)^{-\frac{1}{4}}$$

Notice that for a small cavity length ($w_0 \approx w_1$) the mode volume (V_0) can be estimated as $V_0 = \frac{\pi w_0^2}{2} \cdot l$. For the plane-concave geometry the eigenfrequencies of the system of the cavity modes given by equation 7 do not hold. The stable cavity modes λ_{Nqp} are given by equation 20[2], under the constraint that the round trip phase is equal to $N \cdot 2\pi$ as mentioned earlier.

$$\lambda_{Nqp} = 2 \cdot l(N + (q+p+1)\frac{\cos^{-1}(\sqrt{g})}{\pi})^{-1} = \frac{c}{\Delta\nu_{_{FSR}}}(N + (q+p+1)\frac{\cos^{-1}(\sqrt{g})}{\pi})^{-1} \tag{20}$$

In which $g = 1 - \frac{l}{\mathcal{R}_{M_2}}$, q and p are the transverse Gaussian mode indices and N is the longitudinal mode index. Comparing these equations to equation 12, we see that in the case of a plane-concave Fabry-Perot micro-cavity the resonant modes are not only longitudinal, in addition the mirror curvature introduces transverse Gaussian modes.

Part III
COMSOL Multi-physics

Utilizing physical laws we have the ability to describe the world around us. Post WWII after the invention of the turing machine, we have used computers to gain a better understanding of the physical phenomena which these laws govern. Initially these room filling machine had only a fraction of the computational power available today. Due to the scarcity of resources in the past we could only model these physical law's in isolation and the influence of the laws on each other remained quite the mystery. For these mysteries to unravel research and understanding are required. In order to better understand the plane-concave Fabry-Perot micro-cavity COMSOL will be used. COMSOL is a powerful software which utilizes the solutions of physical laws within small regions to better understand the whole. The elements on which the physical laws are solved are determined by a functional mesh generation which specifies the required size of the element based on the surrounding geometry. Further discussion of the COMSOL software and the manner in which it will be implemented can be found in the next section.

4 Finite Element Analysis

Finite Element Analysis (FEA) has the purpose of reducing the number of models and experiments required to gain a better understanding of physical phenomena. FEA helps efficiently design, optimize and control the devices or processes required in the study of these phenomena. With the ever increasing available computational power this method allows us to find solutions and phenomena which reach beyond our intuitional or analytical approach.

Utilizing the Finite Element Method it is possible to find approximate solutions of the physical law's which describes the world around us. For example conservation laws and the laws which govern the propagation and interaction of electromagnetic radiation. Conveyed in mathematical language these laws are discretized according to the Finite Element Method (FEM), thus allowing for the approximation of the afore mentioned physics. This method is based on numerical analysis of mathematically well posed physical phenomenon. The mathematical language used in the description of these physical laws often come in the form of partial differential equations (PDEs). These equations can often not be solved analytically and thus require a numerical model equation in order to find a solution. This method results in a good approximation of the

physics governing the system we would like to study. None the less in order to gain valuable information form the solutions obtained by this method we are required to analyse the results, hence the term Finite Element Analysis.

Lastly we will look at the process involved in FEA, namely building an 'air-tight' geometry, defining the materials, introducing the domain settings and boundary conditions and lastly defining the correct size for the mesh. In order to simulate a physical phenomenon with the use of FEA the first requirement is the creation of an 'air-tight' geometry. This entails that the system may not have any free space which is not defined to ensure the system may be solved in its entirety. In addition every element used in the building of the geometry needs to be assigned the correct material properties, these are depend on the system which you wish to analyse. Moreover COMSOL has a large library of material and the option for the user to define the material properties. To get an understanding of the physical behaviour of the system the correct the boundaries and domains need to be selected. As last we are required to define a mesh which will determines the size of the discretized mathematical elements. The mesh size is depend on the system under investigation, in our case we will require that the mesh is smaller than the wavelength we want to study to ensure that the system is correctly resolved.

5 Build Progression

Having gained a grip on the theory and having had an introduction to the COMSOL multi-physics environment we now can consider the build progression of the simulation. In order to gain a further understanding of the plane-concave Fabry-Perot Micro-Cavity the goal will be to build a simulation which is in line with the presented theory.

Moreover in order to achieve this it will be important to ensure that we make the right choice for a number of different features in COMSOL. For example the spatial dimension in which we will be simulating. This is important due to the fact that different spatial dimensions will have different geometries and computation times, as one can imagine a full 3D simulation will require significantly more computational power. In addition a 3D simulation would require the physical laws to be solved for significantly more discretized regions result in longer computation time when compared to 2D-axissymmetric or plain 2D simulations.

Lastly we can choose between a number of different modules such as the Radio-Frequency, Wave-Optics or Ray-Optics modules. Furthermore having decided which module best fits our simulation goal we will have to determine

which interface is best for studying our model.

Note that in attempting to build our correct model there have been numerous occasions when the previous model was discarded and the new model was built from scratch. This was in order to ensure that the new model did not have any influence from the earlier model. In the process many parameter had been changed, not only in the geometry of the system. For example there have been many changes in the mesh settings, studies had been adapted multiple times to find the right results and the parameter required to construct the build had been changed most of all. All builds created in the process have been saved

5.1 Spatial Dimension

The best choice for the spatial dimensions is a balance between the computational power required for the simulation and the information obtained from said simulation. The model which would best match the real world physical setup is the 3D build, however this would require large computational power or will result in long processing times. When considering the setup of a plane-concave Fabry-Perot Micro-Cavity it becomes apparent that the model houses symmetry along the centre axis depicted below.

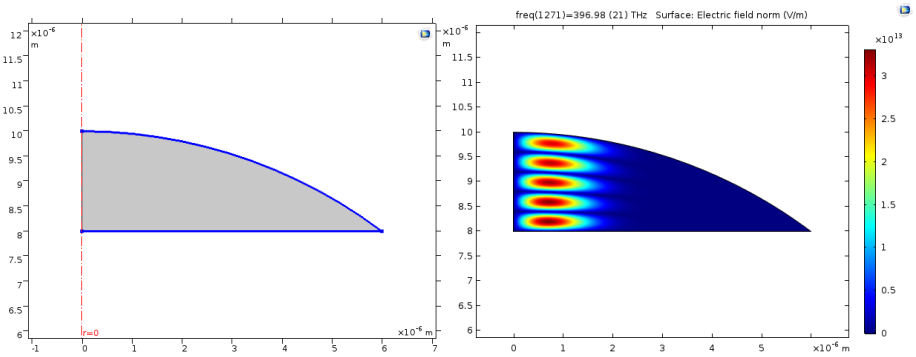

Figure 6: On the left: plane-concave Fabry-Perot Micro-Cavity setup with symmetric axis $r = 0$ and the perfect electric conductor highlighted in blue. Furthermore the interior of the cavity is air. On the right: 2D-axissymmetric build with cavity modes which have no field near the symmetric axis r. Field distribution is shown at 397 [THz].

The fact that the setup is symmetric around the axis allows us to simulate the real world setup with the use of a 2D-axissymmetric build. This would ensure shorter computation times without the loss of any information present in the 3D model. In attempting to build the 2D-axissymmetric build a number

of issues came up mainly the distribution of the electromagnetic field did not match what was expected for the theory.

In the setup of the 2D-axissymmetric build initially the geometry was build off axis, the cavity was built as a 2D model in a 2D-axissymmetric spatial build. This resulted in electromagnetic field distribution which looked nice however this was only due to the boundary conditions and the 2D-axissymmetric nature of the build. The simulation which was preformed was thus a representation of a donut build structure rather than the curved Fabry-Perot cavity we wanted to simulate. To correct this the geometry the 2D-axissymmetric was built in accordance with the spatial nature of the build. In the figure 6 the correct geometry for the 2D-axissymmetric spatial build is shown. We observed resonance modes which had no field distribution in the centre of the cavity which can also be observed in figure 6.

Thus ultimately these discrepancies led to the choice to build the model in the 2D spatial dimension. The simulation could in this case be seen as the cross-section of the 3D model. Adapting the geometry to this setup cavity modes were observed with field distributions which matched the theory. For this reason the choice was made to continue in the 2D spatial dimension in order to complete the desired model setup.

5.2 Module Choice

To gain a better understanding of the various possibilities within COMSOL, we built a number of different pre-made models. These models could be directly loaded into the COMSOL environment. However in order to further understand what was required for the creation of a suitable simulation, we built these models from scratch using the provided material. Which contains the theory of the models and a step by step guide with instructions on how to build the models. The models we built to gain a better understanding are the following:

- Cavity Resonator – Radio-Frequency module
- Cascaded Cavity Filter – Radio-Frequency module
- Fabry Perot – Wave Optics module
- Symmetric Laser Cavity – Wave Optics module
- Distributed Bragg Reflector – Ray Optics module

These models where built using different COMSOL modules and interfaces in order to find which would be suited for the simulation we wanted to build.

The most important was the introduction of the study two methods, namely the eigenfrequency and frequency-domain analysis. The first method of study requires specific settings for the eigenfrequency solver which need to be adjusted in order to find physical solutions to the system. When implementing this method in the plane-concave Fabry-Perot micro-cavity build the resulting eigenfrequencies did not result in physical solution of the system. This was a shame since the study was significantly faster that the parametric sweep across the frequency domain.

Parametric sweep across the frequency domain is the second method which the Fabry-Perot model introduced. The parametric sweep analyzed each frequency individually and thus resulted in many modes which were of no particular interest in the study of the system. In addition it required significantly more processing time when compared to the eigenvalue analysis.

However the use of the parametric sweeps with the goal of finding resonant modes was possible since the field distributions had been determined for every frequency in the sweep, even though the sweeps led to many modes which did not correspond to the expected physical theory. The ability to manually search through the resulting electromagnetic field distributions made it possible to determine the resonant frequencies.

Furthermore in the study of the simple Fabry-Perot system the method for determining the total energy present within the cavity was introduced. Though the method was not ideal in our case since it considered the field intensity throughout the entirety of the cavity and not the intensity of the central region divided by the total intensity in the cavity. None the less this method did allow us to determine the Q-factor of a single mode and the analysis of the total energy across the spectrum.

The symmetric laser cavity was build with the use of the bidirectional Electromagnetic Waves, Beam Envelope interface. As the name of the interface suggests this interfaces deals with the propagation of electromagnetic waves. This model was was useful to gain an understanding of the boundary conditions present in the system and their influence. The boundary conditions could be implemented in such a way that the cavity could be regarded as having been build with perfectly reflecting mirrors. This was achieved due to the implementation of Perfect Electric Conductor, this entails that the fields at the boundaries of the system are defined by:

$$E = E_1 \exp(-j\phi) + E_2 \exp(j\phi). \tag{21}$$

In which E_1 & E_2 are solved for slowly varying field envelopes for the propagating waves in both directions, in addition ϕ represents a rapidly varying

predefined phase factor. The solution method utilized by this model is based on searching for the eigenfrequencies of the system. Moreover utilizing the implementation of a stationary study aiming to solve for both the electric field and the frequencies that self-consistently fulfill the resonance condition.

Furthermore the Beam Envelope interface required an approximation of the electric field in order to make the nonlinear solver converge to the correct mode fields. We aim to find the depiction of the mode fields which are present for certain resonance conditions. Seeing as this interface would require additional theory to be implemented correctly and does not result in additional valuable information when compared to the study method in the Fabry-Perot module. For this reason there was no further implementation of the Beam Envelope interface.

The Distributed Bragg Reflector was built with the aim to find the best manner of implementing the DBR in the cavity system. This model utilized the Ray Optics, Geometrical Optics interface which is an interface that considers the physical properties of ray optics. These ray optics which is useful for the approximation of the paths along which light propagates under different circumstances. Since we aim to find the field distribution under certain resonant circumstances and since the propagation of the rays within the cavity do not require further study. This is due to the fact that the study of the rays within the cavity leads to stability criterion which have already been discussed in the theory.

The Cavity Resonator and Cascaded Cavity Filter were also built however these model utilized the Radio-Frequency module. This module dealt with the physical phenomenon which occur at a significantly larger wavelength than the wavelength required for the study of the plane-concave Fabry-Perot micro-cavity. Due to the insignificance of these models with regards to the understanding of the physical phenomenon present within the plane-concave Fabry-Perot micro-cavity, there was no need for further study of these modules.

The choice was made to use the Electromagnetic Waves, Frequency Domain interface within the Optics>Wave Optics module. The main reasons being that it allowed for the desired study of the system utilizing parametric sweeps over a range of frequencies. Moreover the ability to find the total energy within the cavity was of importance in the final study and classification of the system. Lastly the module choice allowed for the implementation and study of the desired system in a simple yet complete manner.

6 Model Setup

The goal was to build a functioning simulation of a plane-concave Fabry-Perot micro-cavity with the use of Distributed Bragg Reflectors which will function as the highly reflective mirrors. Moreover, we aim to ensure that the resulting data is such that it contains the values of certain parameters, which are required for the characterization of the system.

After having gained an understanding of the different possibilities for spatial dimensions, module choices and methods analysis within the COMSOL software. It is now possible to create the system which meets our design criteria, namely a model which allows the adaptation of the fundamental cavity parameters such as the cavity length, the wavelength of the incoming light and the radius of curvature of the concave DBR system without breaking the geometry. In other words it must be possible to change any one of these fundamental parameters and then construct the build geometry without getting an error. In order to make this possible the geometry of the system must be defined by these parameter and be constructed in such a manner that it is scale-able with every individual parameter.

Furthermore the material setup is important for the properties of the DBRs as the choice of the refractive indices will determine the functionality of the DBR as described by function 17. In addition the

Lastly it is important to consider the study setup of the model. As this is where all the previously mentioned factors come together. In addition the study of the system and the post processing of the data is what will allow us to gain a better understanding of a plane-concave Fabry-Perot micro-cavity. Allowing the visualization of the field within the cavity at physical states and the calculation of the parameter such as the Q-factor, the free spectral range and the finesse. All parameter which characterize a cavity system and thus are of importance in the further development of such cavity interfaces.

6.1 Wave Optics Module

In the previous section we commented on the choice of the module used in the creation of the simulation. Here we will discussed the Wave Optics module with a focus on the advantages we have due to the use of the electromagnetic waves, frequency domain interface within this module. In our case we aim to study a resonant cavity in which is designed to confine the electromagnetic radiation within the cavity. In addition to being interest in the intensity within the air-gap between the DBR's, the distribution of the electromagnetic radiation is of interest in the study of this system. Our aim is to find the Gaussian modes

which can be found through the analysis of the cavity response to the a range of specific frequencies. These frequencies are given by the resonant conditions derived in equation 7.

In addition the aim is to build a simulation which is as close as possible to a plane-concave Fabry-Perot micro-cavity build in the real multi-physics world. An important feature in the electromagnetic waves, frequency domain interface is that due to the assumption that we are dealing with resulting fields which are "wave-like" (power transfer occurs mainly through radiation). The enables the implementation of boundary conditions such as Scattering Boundary Condition and Perfectly Matched Layers, which are used to model the boundaries the system has to free space.

6.2 Model parameters

In building the system a number of parameters have been introduced in order to meet the requirement of a full tune-able system. In which the design parameters do not break the geometry that has been constructed with the uses of these parameters. The parameters can be categorized in two different groups, namely the design parameters and the control parameters.

The design parameters are adjustable and define the geometry of the system. In addition they define a number of the control parameters, such as the distance of the air-gap and the resonance wavelength for a given N. The design parameters are listed in the table below,

Name	Expression	Description
Lambda_0	935 [nm]	Design wavelength
Lambda_max	700 [nm]	Maximum sweep wavelength
Lambda_min	580 [nm]	Minimum sweep wavelength
N	3	Resonant mode order
n_L_H	3.5	High refractive index of the lower Bragg pair
n_L_L	2.7	Low refractive index of the lower Bragg pair
n_U_H	3.5	High refractive index of the upperBragg pair
n_U_L	2.7	Low refractive index of the upper Bragg pair
R_0	10 [um]	Radius of curvature of the upper DBR

Table 1: The design parameters of the plane-concave Fabry-Perot micro-cavity. Note the expression given are based on the design parameters used in Cavity Build 6.1.1.

Furthermore the choice to split the refractive indices of the different Bragg pairs in to upper and lower in addition to the differentiation of higher and lower indices was implemented in order to allow the adaptation of the system.

To allow the choice for different Distributed Bragg Reflectors on the top and bottom. The design parameters are the most important this becomes clear when considering table 6.2, as all the control parameters have been defined by the aforementioned design parameters.

Name	Expression	Description
c	299792458 [m/s]	Speed of light
d_airgap	(d_sidegap+d_U_L)	Distance of the air-gap
d_L_H	Lambda_0/(n_L_H*4)	Distance lower mirror (high n)
d_L_L	Lambda_0/(n_L_HL*4)	Distance lower mirror (low n)
d_sidegap	Lambda_0-d_U_L	Distance of the side gap
d_U_H	Lambda_0/(n_U_H*4)	Distance upper mirror (high n)
d_U_L	Lambda_0/(n_U_L*4)	Distance upper mirror (low n)
f_0	c/(d_airgap)	Design frequency
f_max	c/(Lambda_min)	Maximum sweep frequency
f_min	c/(Lambda_max)	Minimum sweep frequency
f_resonance	(c*N)/(2*d_airgap)	Resonance frequency
lam_resonance	c/f_resonance	Resonance wavelength

Table 2: The control parameters of the plane-concave Fabry-Perot micro-cavity. Note the expression given are based on the design parameters used in Cavity Build 6.1.1.

The parameter defined above are implemented in the geometry of the setup. They have been design in such a way that the resulting geometry is scale-able to the design parameters.

6.3 Geometry and Mesh

The next step in the setup is the geometric build of the plane-concave Fabry-Perot micro-cavity. In the process of creating the geometry which met the design criteria a number of problems were encountered. As was mentioned in the previous section the geometry is built in a spatial dimension. This has a large influence of the behavior of the physical phenomenon which we wish to describe. For example the resonance modes that were found in the 2D-axissymetric models did not have a fundamental Gaussian mode profile.

Moreover these results were not analyzed in detail and thus they could be interpreted as first order Hermite-Guassian mode, a depiction of the different Hermite-Guassian modes in shown in figure 6.3. The mode that we could attribute to the cavity would be the (1,0) Hermite-Gaussian mode as the fundamental mode whereas the mode depicted in figure 6 would correspond to the (1,5) Hermite-Gaussian mode. The mode that we are interested in was the

fundamental Gaussian mode. Since it was not possible to find this mode, the 2D-axissymetric geometry build could be discarded. This led to the choice of the 2D spatial dimension for the model build.

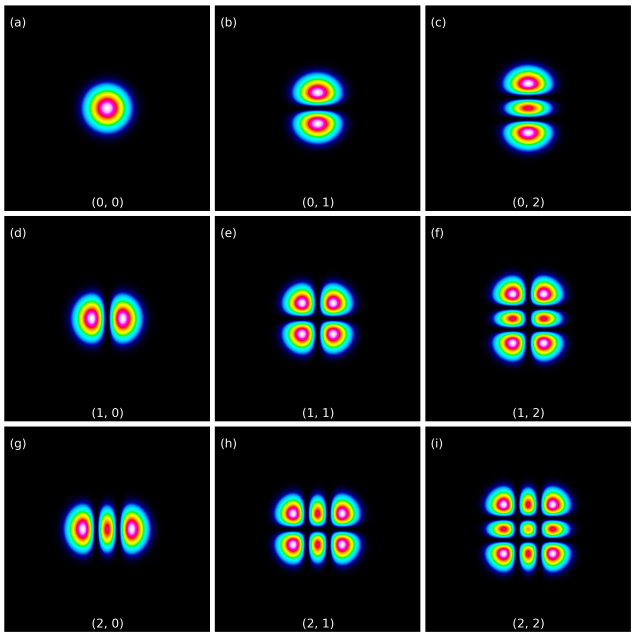

Figure 7: An array of subplots containing the various Hermite-Gaussian modes. Notice that the definition of beam width becomes fairly abstract in the higher-order modes.[14]

The initial 2D build was rather simple to construct, this was mainly due to the fact that this build did not yet implement the Distributed Bragg Reflectors. The highly reflective mirrors required for a Fabry-Perot cavity were implemented with the use of 'Perfect Electric Conductor' boundaries. These boundaries have been described in the previous section. Due to the uses of the boundaries the only requirement for the geometry of the build was a circle and a rectangle. The rectangle would cut-off the circle at the top, their intersection would result in a curved cavity with perfect reflecting mirrors. Since it was critical that the wavelength of the incoming light fit within the cavity it is important to discuss the defining cavity parameter. The thickness (d) of the rectangle which in turn is also the cavity length and as such the defining parameter of the cavity resonance. The geometry of the build will not be discussed in more detail. It is

a simple model which does not come close to any system that could be realized in a lab environment due to the fact that it utilizes PEC which have not been found to exist in reality. An example of this mode can be found in figure **??**.

After the creation of a successful 2D cavity build with PEC boundaries, the next step was the implementation of the Distributed Bragg Reflectors in the geometry of the build. This resulted in more issues in the creation of a scaleable geometry. The main complication was the fact that every region needed to be defined such that they different region within the system would line up perfectly. Any discrepancy in the geometry which resulted in a minor overlap of different regions would result in complication in either the creation of the mesh or in defining material properties to the regions. The basis of the curved DBR geometry was the same as in the perfect 2D-build, namely a circles and a rectangles. However the in this build it was not just a simple intersection between a rectangle and a circle. The build was made with the uses of 10 rectangles, 5 circles, 3 geometric region unions, 4 geometric region arrays and 7 geometric region differences. The result geometric build is shown in figure 6.3.

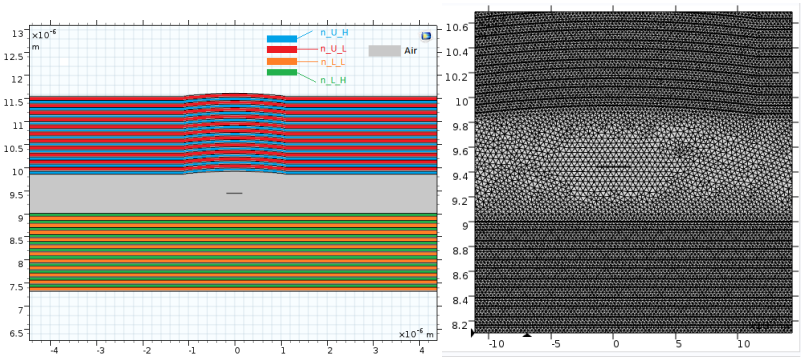

Figure 8: On the left: Geometry of a plane-concave Fabry-Perot micro-cavity setup in the 2D spatial dimension constructed with Distributed Bragg Reflectors. Cavity length of this geometry is 935 [nm], radius of curvature DBR is 10 [um]. On the right: A zoom of the mesh of the system. Screenshots from COMSOL build 6.1.0.

In addition the implementation of the Distributed Bragg Reflectors resulted in issues concering the creation of the mesh for the build as mentioned in the previous paragraph. Up until this build the mesh had not resulted in any issues and was mostly overlooked in earlier build. None the less this is a fundamental part of the FEA, in other words issues in the mesh will result in issues in the ability to properly analyse the system and gain valuable results. The issues in the mesh arose mostly in the intersection and overlap of certain regions which

had been define by the geometry. The main issue was due to the initial overlap of narrow regions in which the mesh was significantly over-defined. An over-defined mesh will result in longer processing times due to fact that significantly more elements needed to be analyzed. This issue was solved by eliminating the interior boundaries in these regions.

Moreover it is of equal importance to ensure that mesh is not to coarse or under-defined as this would in turn lead to the loss of data. Thus the choice was made to define the mesh on the basis of our knowledge of the system instead of allowing the COMSOL software to define the mesh. In the defining of the mesh it is important to ensure that the mesh size is smaller than the design wavelength (λ_0). However it is also important to not define the mesh to be to small as this would increase the processing time without resulting in additional useful information.

6.4 Material Setup

In the COMSOL software it is possible to attribute different material to different regions defined by the geometry. The main region where the material is relevant is in the Distributed Bragg Reflectors. This is due to the fact that these reflectors are made up of different the Bragg pairs with varying refractive indices. In a lab environment a common choice of material for these Bragg pairs are AlAs($\lambda/4$)/GaAs($\lambda/4$). These materials form a splendid DBR setup with high reflectivity however there are still a number of limitation such as for example the wavelength dependence of the material. As can be seen in the description of the geometry and the parameters our cavity has been built with constant refractive indices for all wavelength. This is not the case in a real setup due to the aforementioned wavelength dependence for that reason the simulation has certain limitations in achieving a simulation of the plane-concave Fabry-Perot micro-cavity which is as close reality as possible.

In the future implementation of the build it would be possible to define the materials which are used in the construction of the Bragg pairs. This has not been implemented in the current build due to the fact that omitting the wavelength dependance of these materials results in a minor deviation for the realistic system. However the aforementioned deviation does not pose a major issue in the creation of a functioning and tune-able micro-cavity. Furthermore the implementation of a parameter which depends on the wavelength would further increase the processing time when running the simulation. Thus the choice had been made to build the model with Bragg pairs with constant material properties, such as the refractive index.

For a COMSOL build to function it is required that all regions in the build

have the correct materials assigned to them. The overlapping regions in the earlier builds thus resulted in many small regions which all needed to have materials assigned. This was also solved by the elimination of interior boundaries within these regions.

6.5 Study

Initially we attempted to solve the model as an eigenvalue problem. This requires that we the frequency range in which to search for the eigenfrequencies and in addition the number of eigenfrequencies for which we aim to find the eigenvalue problem solution. The reason this was the desired study method was due to the fact that it would allow us to only evaluate the system at the frequencies which we are interested in, namely the resonance frequencies. However in the study of the simple 2D model build the uses of this study option resulted in frequencies which were not resonant modes of the system and thus also not the solution to the eigenvalue problem we aim to solve. For that reason this study method was not utilized further in the build progression.

Instead the choice was made to proceed with the parametric sweep. The parametric sweep solves the model for each frequency in a specified range. This approach has several drawbacks compared to the eigenvalue study method. The most significant draw is the fact that the parametric sweep requires the manual examination of each mode. Many of the modes will be nonphysical and as such will not contain any relevant information. Thus this method will require prior knowledge of the frequencies at which resonant modes are expected. In the case of our model the theory for the resonant modes as been discussed in depth. Thus we having an expression for the frequency of the resonant modes we can limit the number of frequencies for which we will be required to manually inspect, in the search for resonant modes.

The parametric sweep also has a major advantage namely that the cavity response is analyzed for a range of frequencies. Utilizing this data is becomes possible to create the spectrum of the cavity. The study of this spectrum can determine the characterizing values such as the finesse, the free spectral range or the Q-factor. In the case of the Q-factor the only requirement is to find the response of the system at a resonance frequency. Considering equation 15 in order to determine the Q-factor we need to find a resonant frequency (ν_N) and the FWHM ($\Delta\nu_{FWHM}$) at this frequency. If the Q-factor for a specific frequency is known it is a simple to determine the finesse. Again considering equation 15, we find that the finesse can be expressed as $\mathcal{F} = \frac{Q}{N}$.Lastly we would like to determine the free spectral range ($\Delta\nu_{FSR}$), in order to determine this characterizing parameter analyzing the spacing between resonant modes

will be required. In order to find multiple resonant modes on the spectrum it will be necessary to expand the frequency range under consideration.

Part IV
Results

7 2D Perfect Electric Conductor model

Initially we will discus the results from the 2D 'Perfect Electric Conductor' (PEC) model. The geometry of the model and the field distribution for the fundamental Gaussian mode, the (0,0) Hermite-Gaussian mode are shown in figure 9. It is easy to see that this model is a good representation of the theory which has been described. For example the mode within the cavity is clearly a Gaussian mode, which is what can be expected from the theory. This model is a ideal simulation this is due to the PEC boundary conditions. Which impose that the electric field go to 0 at the boundaries, this results in boundaries with perfect reflection. There are two aspects of this build which would not hold in the real multi-physics world, namely the existence of a perfect electric conductor and the excitation of the cavity from within.

In reality a perfect electric conducting material is yet to be found. None the less there have major strides in the creation of materials or composites which allow for very high reflection. An example of such a construction is are the distributed Bragg pairs which have been used in the final model.

Furthermore the excitation from within is also not a correct representation of the system we would like to simulate. As the aim would be to find the response of a cavity which is excited by laser light. In the case that we would be able to make a cavity with perfect electric conducting boundaries and we attempted to excite that cavity with laser light. The light would not be able to enter the cavity since the boundary is perfectly conducting and thus perfectly reflecting. Thus be no propagation within the cavity and no resulting field.

Moreover it becomes clear that we do not wish to have a PEC boundary in the system due to the issues discussed above. Thus the implementation of the distributed Bragg reflectors is beneficial.

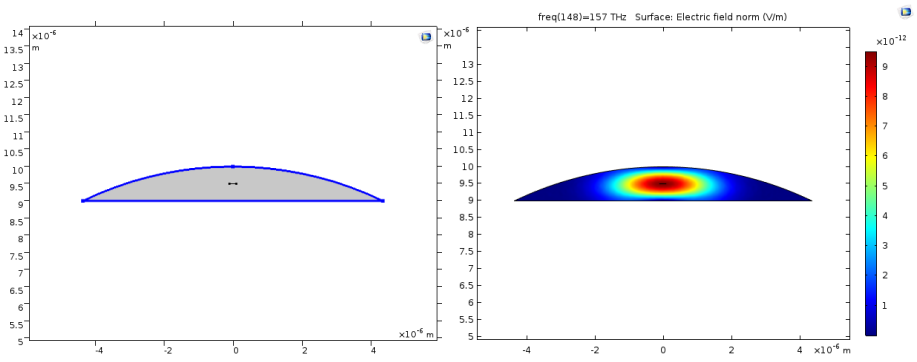

Figure 9: On the left: Plane-concave Fabry-Perot micro-cavity setup in the 2D spatial dimension. The radius of curvature of the mirror is 10 μm and the cavity length is 1 μm.The perfect electric conductor highlighted in blue. Furthermore the interior of the cavity is air. On the right: 2D build with the fundamental Gaussian mode of order $N = 1$. Field distribution is shown at 157 [THz].

Lastly having constructed a cavity which has been described as a perfect match to the system it is rather interesting to confirm whether the results found match the theory which has been given. In order to check this we will use equation 7. The length of the cavity is 1 μm. Thus we find $\lambda_1 = 2\mu m$, keeping in mind that $\nu_N = \frac{c}{\lambda_N}$ we find that $\nu_1 = 149.9THz$. This is a slight deviation from the theory, however the theory is not for a curved mirror. Considering equation 20 we find $\nu_1 = 165.2THz$. Thus neither of these perfectly describe the 2D PEC model. None the less they are both close to the determined value and are both derived under the consideration that the mirrors are not perfectly reflecting, this could cause the discrepancy.

8 2D Distributed Bragg Reflector model

After having considered the functioning 2D PEC model, the next model under consideration will be the 2D model in which the PEC boundary conditions have been replaced by distributed Bragg reflectors. This model had a number of interesting results, firstly an analysis of the spectrum of total energy within the cavity will be determined. After which different mode will be taken under consideration. The aim will be to characterize the modes of the cavity according attempting to find the free spectral range ($\Delta\nu_{_{FSR}}$), the finesse ($\mathcal{F}$) and the Q-factor.

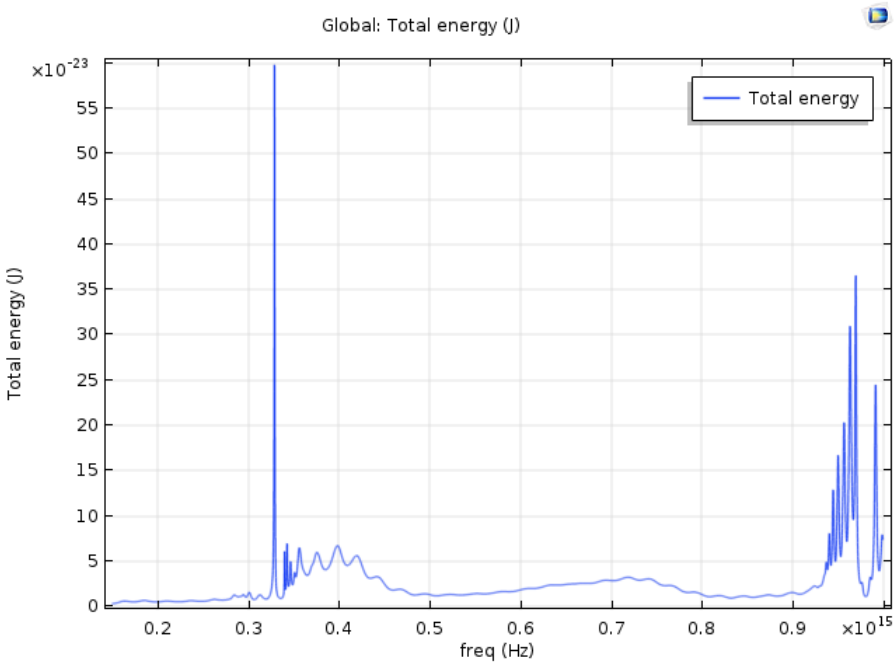

Figure 10: The spectrum of the total energy within the cavity. Build 6.1.0

8.1 Characterizing the 2D Distributed Bragg Reflector model

8.1.1 Free Spectral Range

Firstly we will attempt to determine the free spectral range ($\Delta\nu_{FSR}$). In order to determine the free spectral range we will need the spectrum of the cavity shown in figure 10. Considering this spectrum it is apparent that there is only one clear resonance peak. This is odd seeing as equally spread peak would be expect in the spectrum.

In principle the aim would be to normalize the cavity and in doing so emphasize the resonance peaks. This would be done by integrating the intensity over a certain region within the cavity, namely the center of the cavity, and dividing this by the intensity integration of all regions.

However in the attempts to achieve this it became apparent that the source was a major contributor to the total energy within the cavity. Since the source was located in the center of the cavity, it was not possible to normalize the spectrum with the use of surface integration over this region. Through out the progression of the simulation the source resulted in serval issues.

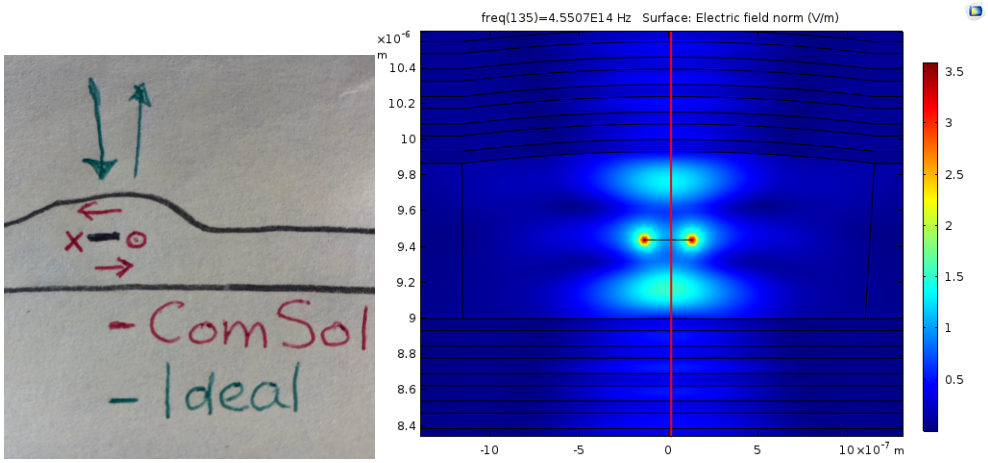

Figure 11: On the left: A sketch of the different possibilities for the simulation of the electric field excitation from within the system shown in red. Furthermore the ideal lab scenario is shown in green. On the right: Illustration of the unexpected electric-field contribution at the edges of the source.

In the attempts made to circumvent these issues, it became clear that it would not be possible to simulate the laser-light from an external source interacting with the system. In figure 11 an example of the unwanted excitation of the electric field at the edges of the sources is shown. In addition the figure illustrates the possibilities for defining the electric field within COMSOL compared to the ideal scenario which we would find in a lab setup. The issues with the source have not been resolved completely, in order for the model to reduces the unphysical phenomenon it will be of large importance to revise the source.

In order to compare the numerical simulations to the theory equation 7 will be used. The length of the cavity is 935 nm. Thus ν_2= 320.6 [THz] is determined as resonance frequency for the integer value N=2. This is a slight deviation from the theory, however the theory is not for a curved mirror. Considering equation 20 ν_{200} = 342.9 [THz]. Thus neither of these perfectly describe the plane-concave Fabry-Perot micro-cavity model. None the less they are both close to the determined value and thus in improving the simulation could help get these numerical values closer to the analytic solutions.

8.1.2 Q-factor

None the less upon inspecting the largest resonance peak it corresponds to the 2nd order fundamental Gaussian mode. In terms of the Hermite-Gaussian mode this would be (0,1). This mode is depicted in figure 12, in addition the cross-

section of the cavity intensity profile through the center of the cavity can be seen. Upon inspecting the cross-section a clear intensity profile which matches what is expected from the theory is found. Furthermore just as in the PEC model the Gaussian profile of the electric field can be observed. Having found a nice mode which is in accordance to the theory, the next step is the characterization of this mode.

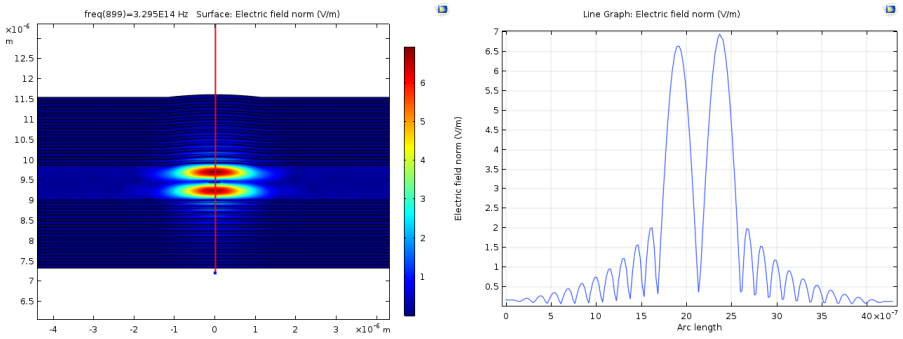

Figure 12: On the left: Plane-concave Fabry-Perot micro-cavity setup in the 2D spatial dimension constructed with Distributed Bragg Reflectors. These reflector consist of 11 Bragg pairs. The fundamental Gaussian mode of order $N = 2$. Field distribution is shown at 329.5 [THz]. On the right: The cross-section of the intensity profile along the red line shown within the cavity.

In order to determine the the Quality factor of the resonance peak in the spectrum shown in figure 7 a zoom will be required. A zoom of the spectrum can be achieved with two different methods, zooming in on the existing spectrum to gain more detail of the resonance peak or reevaluating the system over a smaller frequency with a smaller step size in frequency. Both method have been applied in the search for the Q-factor. The result of the zoom methods is shown in figure 13.

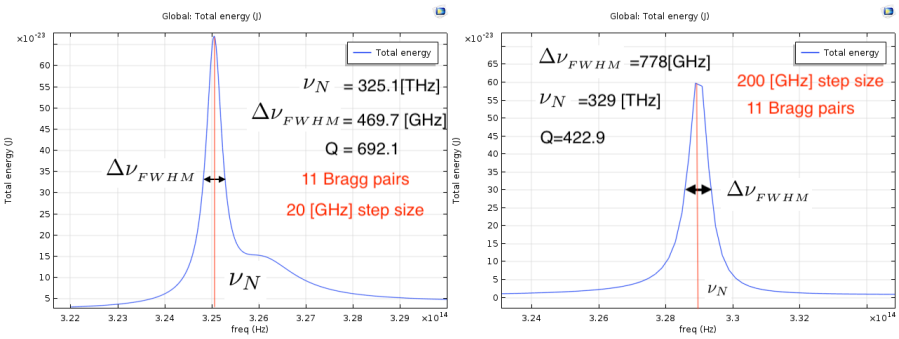

Figure 13: On the left: The spectrum of the total energy within the cavity. Build 6.1.1 – Zoomed in on $N = 2$. Frequency sweep step size 20 [GHz]. With 11 Bragg pairs on each side of the cavity; On the right: The spectrum of the total energy within the cavity. Build 6.1.1 – Zoomed in on $N = 2$. Frequency sweep step size 200 [GHz]. With 11 Bragg pairs on each side of the cavity.

Important to note is the fact that the Q-factor determined with a zoom of the already existing spectrum is a very crude approximation. The value obtained does not represent the Q-factor of the system which the theory would predict. Due to the peak clearly being cut-off at the peak due to a lack of data points. An attempt was made to fit the curve to a Lorentz distribution, which is often the description of spectral lines and thus a close fit to the observed curve would be expected. However in fitting the data point to this curve it became clear that they did not perfectly fit the Lorentz distribution. The reason for this discrepancy later became clear when reevaluating with smaller step-size.

Notice that the resonance peaks obtained with the different zoom methods are significantly different. Firstly in the reevaluation of the system over a smaller frequency with smaller step size a side-lobe becomes apparent. This was an artifact which was not present in the original spectrum. Moreover the present of the side-lobe could be an explanation for the imperfect matching of the data to the Lorentz distribution. In order to find the cause of this side-lobe more further analysis would be required. None the less the expectation is that it is an artifact of the simulation and not caused by a physical phenomenon.

The reason the analysis of the Q-factor is still given in figure 13 is due to the fact that in the next section an analysis has been made with the same step size but with additional Bragg pairs to further increase the reflectivity of the system in and doing so also further increase the finesse. In order to compare the results effectively the analysis method for both peaks will be the same.

8.1.3 Finesse

Furthermore the Q-factor found in the section above can be compared to analytic calculation. This is due to the relation of the Q-factor and the finesse given in equation 15. In order to determine the finesse of the system we will need to determine the reflectivity ($R = |r^2|$). Which can be determined with equation 17 and the definition of the finesse: $\mathcal{F} = \pi\sqrt{R}/(1-R)$.

To determine the finesse of the system the reflectivity of the mirrors must be known. Equation 17 analytically determines the reflectivity of the setup. Knowing all the refractive indexes an easy calculation based on 11 Bragg pairs show the reflectivity R is equal to 0.986827. This a high reflectivity non the less it can be increased simply in the simulation by extending the arrays which determine the number of Bragg pairs. This analysis is given in the next section.

Now knowing the reflectivity of the setup the definition of the finesse given above shows that the finesse of the system constructed with 11 Bragg pairs is 236.9. This is not a very high finesse and thus the increasing of the number of Bragg pairs is important to determine whether this system could result in a high finesse cavity.

The finesse can be utilized together with the free spectral range to determine the full width half maximum. However due to the crude data of the numerical simulation and the artifacts which are not assumed to be representations of physical phenomenon the further comparison of the analytically determined finesse has been omitted.

8.2 Optimizing the 2D Distributed Bragg Reflector model

To further increase the Q-factor it is possible to add additional Bragg pairs. As mentioned in above this would further increase the reflectivity of the mirror's. As a consequence will ensure that the FWHM will decrease further. With the result that the Q-factor will increase.

Equation 17is again used to analytically determines the mirrors reflectivity. Knowing all the refractive indexes an easy calculation based on 22 Bragg pairs show the reflectivity R is equal to 0.999956.

Now knowing the reflectivity of the mirrors the definition of the finesse given in the previous section shows that the finesse of the system constructed with 22 Bragg pairs is $7.15{\cdot}10^4$. This is a significant increase in the finesse of the system. This proves that the distributed Bragg reflectors in the setup behave as the theory predicts and allow for higher resolution analysis of the system.

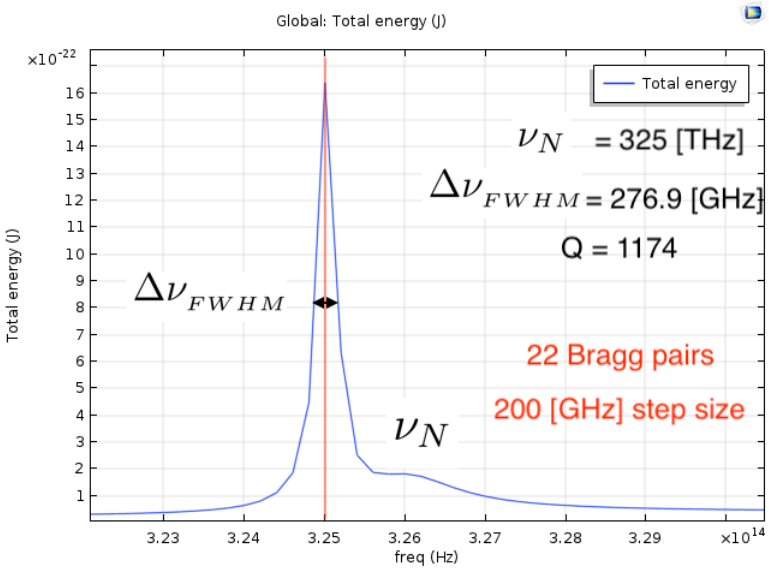

Figure 14: The spectrum of the total energy within the cavity. Build 6.2.0 – Zoomed in on $N = 2$. Frequency sweep step size 200 [GHz]. With 22 Bragg pairs on each side of the cavity.

From the figure above we can see that increasing the finesse of the system results in an resonance peak which is comparable to the resonance peak which was found when decreasing the step size of the frequency sweep. Notice that just as the peak has shifted in to the same resonance frequency observed when decreasing the step size. It will require further study to determine the reason of this shift. Moreover the simulation could be further improved upon to ensure that we find the resulting field of physical phenomenon and not possible artifacts in the simulation.

8.3 Higher-order Modes

Lastly there are a number of higher order modes which can be found. These are shown in figures 15, 16, 17 and 18. No further analysis of these modes has been attempted. Mainly due to the fact that they did not display clear resonant peaks in spectrum shown in figure 10. In addition the attempts to find the resonance peaks of these modes through the method of reevaluation did not result in resonance peaks. Rather we found a smoothed and slightly shifted spectrum compared to the large frequency spectrum. The figures below show the field distributions at the resonance frequencies determined by equation 7. Furthermore the cross-section of the cavity intensity profile through the center

of the cavity is also given for each resonant frequency.

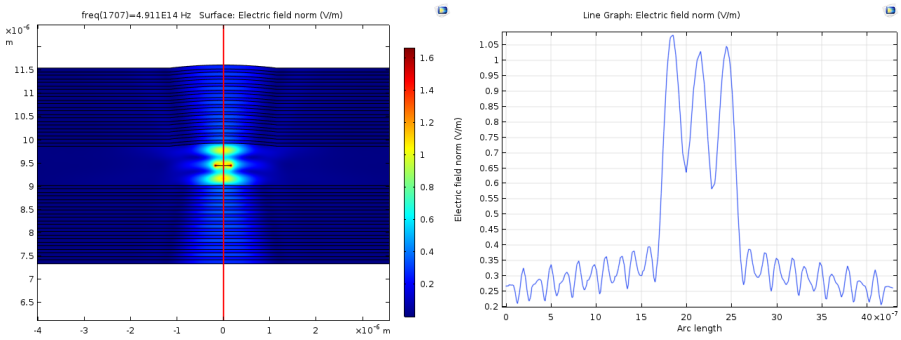

Figure 15: On the left: Plane-concave Fabry-Perot micro-cavity setup in the 2D spatial dimension constructed with Distributed Bragg Reflectors. These reflector consist of 11 Bragg pairs. The fundamental Gaussian mode of order $N = 3$. Field distribution is shown at 491.1 [THz]. On the right: The cross-section of the intensity profile along the red line shown within the cavity.

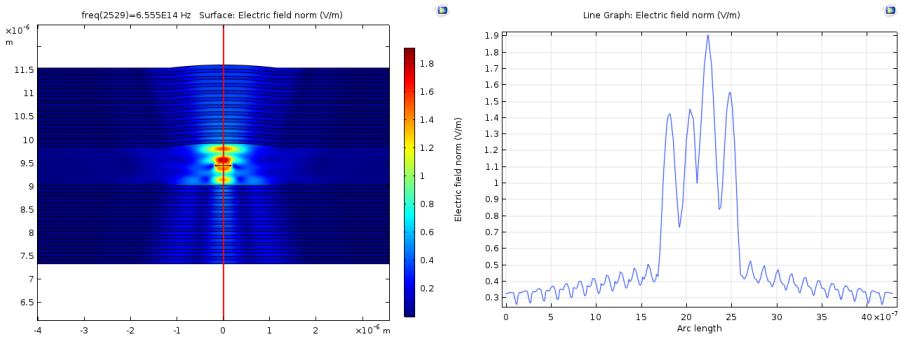

Figure 16: On the left: Plane-concave Fabry-Perot micro-cavity setup in the 2D spatial dimension constructed with Distributed Bragg Reflectors. These reflector consist of 11 Bragg pairs. The fundamental Gaussian mode of order $N = 4$. Field distribution is shown at 655.5 [THz]. On the right: The cross-section of the intensity profile along the red line shown within the cavity.

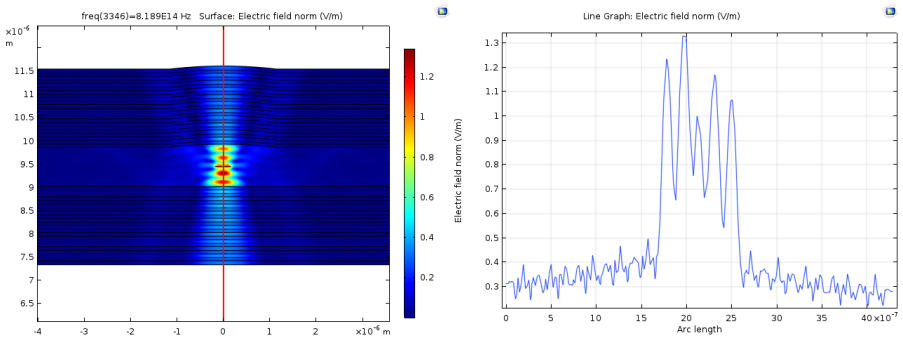

Figure 17: On the left: Plane-concave Fabry-Perot micro-cavity setup in the 2D spatial dimension constructed with Distributed Bragg Reflectors. These reflector consist of 11 Bragg pairs. The fundamental Gaussian mode of order $N = 5$. Field distribution is shown at 818.9 [THz]. On the right: The cross-section of the intensity profile along the red line shown within the cavity.

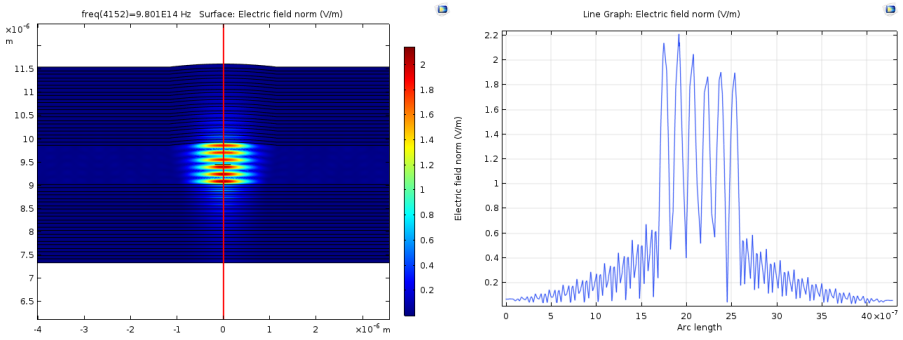

Figure 18: On the left: Plane-concave Fabry-Perot micro-cavity setup in the 2D spatial dimension constructed with Distributed Bragg Reflectors. These reflector consist of 11 Bragg pairs. The fundamental Gaussian mode of order $N = 5$. Field distribution is shown at 980.1 [THz]. On the right: The cross-section of the intensity profile along the red line shown within the cavity.

Considering the field distribution found for resonant modes which correspond to higher values of the integer value N in equation 7. Note that the field distribution should have an egg shaped field distribution shown in figure 19. This field distribution can be observed in both the field distribution for the values N=2 & N=6. In addition note that these modes are also precent when considering the peaks in the spectrum. The resonance peak for N=2 is the most clear, the peak for N=6 is better disguised a the edge of the spectrum. Upon further inspection of the spectrum a clear peak is observed at 979 [THz] which

is close to the mode for the field distribution.

In order to compare the numerical simulations to the theory equation 7 will be used. The length of the cavity is 935 nm. Thus ν_6= 961.9 [THz] is determined as resonance frequency for the integer value N=6. This is a slight deviation from the theory, however the theory is not for a curved mirror. Considering equation 20 ν_{600} = 984.1 [THz]. Thus neither of these perfectly describe the plane-concave Fabry-Perot micro-cavity model. None the less note that in this case equation 20 is a more accurate prediction of the resonance frequency determined in the numerical simulation.

The other modes predicted by equation 7 do not show the expected field distribution and thus it would not be expected that these modes are representations of true physical phenomenon.

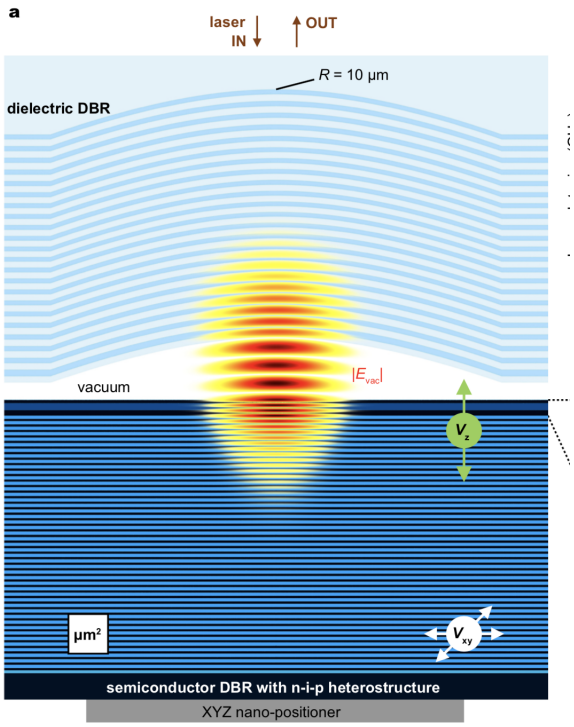

Figure 19: Expected field distribution in a plane-concave Fabry-Perot micro-cavity setup. [15]

Part V
Summary and Outlook

A plane-concave Fabry-Perot micro-cavity model within COMSOL has been built. This model is based on a number of design parameter which can be changed freely without breaking the geometry of the system. The curvature and cavity length can be freely chosen, in addition it is possible to adapt the distributed Bragg reflectors. The design parameters, geometry and mesh of the 2D model have been successfully implemented and meet the design criteria.

In order to improve the model in the analysis of the physical phenomenon within the cavity and important factor to consider is the placement of the source within the cavity, due to the fact that the location of the electro-magnetic field source has not been incorporated as it would be in the lab. Where the excitation of the cavity would be achieved with an exterior laser. This could be improved upon.

Furthermore in order to improve the model in the analysis of the cavity setup in a lab, the system could be build in the 3D spacial dimension. Lastly the study of the system could be improved, currently frequency sweeps are the method of study. This could be optimized and the study could determine the physical mode which are of interest through the solution of an eigenfrequency solver within COMSOL.

The solution of analytic model which describe the system had determined the resonant frequencies. In the study of the model with the use of a frequency sweep a number of resonant modes were found. Considering the field distributions observed at these resonant frequencies there were two mode which displayed the expected field distribution [15].

The modes corresponding to the integer value N=2 & N=6 displayed modes which mostly likely describe physical modes. In addition to the correct field distributions, they also display resonant peaks in the spectrum of the 2D model. These modes were compared to the analytic model. Moreover the mode N=2 was characterized and the finesse and Q-factor were found.

In the future this build could be adapted and implemented to aid in the understanding of plane-concave Fabry-Perot micro-cavities. Which will be built and studied in the Quantum Optics group at Leiden University.

References

[1] R. P. Feynman, *Simulating physics with computers*, International Journal of Theoretical Physics, **21**, 467 (1982).

[2] L. Greuter, S. Starosielec, D. Najer, A. Ludwig, L. Duempelmann, D. Rohner, and R. J. Warburton, *A small mode volume tunable microcavity: Development and characterization*, Applied Physics Letters **105**, 121105 (2014).

[3] G. Brooker, *Brooker - Modern classical optics*, Oxford University, 2003.

[4] Geek3, *Fabry-Perot transmission*, Retrieved March 3, 2019, from https://commons.wikimedia.org/wiki/File:Mplwp_Fabry-Perot_transmission_Fi.svg (2014).

[5] D. J. Klotzkin, *The Optical Cavity*, Introduction to Semiconductor Lasers for Optical Communications , 147 (2013).

[6] S. Bogdanović, *Diamond-based Fabry-Perot microcavities for quantum networks*, PhD thesis, 2017.

[7] L. E. Greuter, *Self-assembled quantum dots in a fully tunable microcavity*, page 125 (2015).

[8] D. I. Babic and S. W. Corzine, *Analytic Expressions for the Reflection Delay, Penetration Depth, and Absorptance of Quarterwave Dielectric Mirrors*, IEEE Journal of Quantum Electronics **28**, 514 (1992).

[9] C. J. R. Sheppard, *Approximate calculation of the reflection coefficient from a stratified medium*, Pure and Applied Optics: Journal of the European Optical Society Part A **4**, 665 (1995).

[10] O. Svelto, *Principles of Laser*, volume 1, 2008.

[11] A. Yariv and P. Yeh, *Photonics: Optical Electronics in Modern Communications (The Oxford Series in Electrical and Computer Engineering)*, Oxford University Press, Inc., New York, NY, USA, 2006.

[12] Anthony E. Siegman, *Lasers*, 1986.

[13] J. P. Landry, *Appendix F : Waist Radius Measurement of Gaussian Beams*, page 477.

[14] L. Hofer, *Higher-order Transverse Modes*, Retrieved from DataRay website: https://www.dataray.com/blog-m2-high-order-modes.html (2016).

[15] D. Najer, I. Söllner, P. Sekatski, V. Dolique, M. C. Löbl, D. Riedel, R. Schott, S. Starosielec, S. R. Valentin, A. D. Wieck, N. Sangouard, A. Ludwig, and R. J. Warburton, *A gated quantum dot far in the strong-coupling regime of cavity-QED at optical frequencies*, (2018).